



Politecnico
di Bari

Repository Istituzionale dei Prodotti della Ricerca del Politecnico di Bari

Environmental monitoring in the Mar Grande basin (Ionian Sea, Southern Italy)

This is a post print of the following article

Original Citation:

Environmental monitoring in the Mar Grande basin (Ionian Sea, Southern Italy) / De Serio, Francesca; Mossa, Michele. - In: ENVIRONMENTAL SCIENCE AND POLLUTION RESEARCH INTERNATIONAL. - ISSN 0944-1344. - STAMPA. - 23:13(2016), pp. 12662-12674. [10.1007/s11356-015-4814-y]

Availability:

This version is available at <http://hdl.handle.net/11589/60259> since: 2022-06-22

Published version

DOI:10.1007/s11356-015-4814-y

Publisher:

Terms of use:

(Article begins on next page)

Environmental monitoring in the Mar Grande basin (Ionian Sea, Southern Italy)

Francesca De Serio and Michele Mossa

DICATECh, Department of Civil, Environmental, Building Engineering and Chemistry, Technical University of Bari, Via E. Orabona 4, 70125 Bari, Italy

Abstract

Hydrodynamic and water quality data has been recorded since February 2014 by a meteoro-oceanographic station installed in the inner part of the Gulf of Taranto, in the north-eastern part of the Ionian Sea (Southern Italy). This monitoring action, managed by the research unit of the Technical University of Bari, DICATECh, Department, could play a pivotal role in a vulnerable and sensitive area, affected by massive chemical and biological pollutant discharges due to the presence of heavy industry and intense maritime traffic. Monthly trends of winds, waves, currents, and biochemical parameters, such as dissolved oxygen, chlorophyll, and turbidity, are analyzed and discussed. The analysis exhibits that the wave regime is slightly controlled by wind forcing; rather, topography strongly affects the wave propagation direction. Surface currents appear wind induced in the measuring station, while near the bottom a quasi-steady current directed towards southwest is formed. The selected water quality indicators show monthly trends consistent with the typical seasonal convective fluxes and mixing.

Keywords: Coastal monitoring . Water quality indicators . Coastal currents

Introduction

The protection of coastal communities and ecosystems, which are strongly affected by climate change and human activities, is one of the main aims of the environmental policy. Therefore, the safeguard of some vulnerable and sensitive coastal sites, such as the Mar Grande basin, located in the inner region of the Ionian Sea in Southern Italy (Fig. 1) and subjected to the presence of heavy industry and anthropic pressure, should be always guaranteed. To this purpose, a continuous monitoring action of the principal hydrodynamic and biochemical parameters in the target area could be a useful managing tool, possibly in conjunction with the numerical modelling. In fact, on one side, collecting a large amount of data in widespread areas is challenging because of technical and economic limitations. Moreover, field measurements are

often limited in time and space (Mossa 2006). On the other side, numerical models represent a more rapid and a less expensive solution, simulating the hydrodynamics and the transport of tracers in extended areas with the desired level of accuracy and in a relatively short time. Nevertheless, in order to be accurate, models need to be calibrated and successively validated by field measurements (Scroccaro et al., 2004; De Serio et al., 2007; De Serio and Mossa, 2014c). Therefore, field information is strongly desirable and even more expected, because it represents a useful support for the local authorities in coastal management and protection.

The target area described in the present work is characterized by a composite topography and is considered highly vulnerable, being exposed to urban and industrial discharges as well as to an intense naval traffic (Di Leo et al., 2013). It embeds the Mar Grande basin (surface area about 35km² and maximum depth about 35m) and the inner basin called Mar Piccolo, formed in turn by two embayments, respectively named I Bay and II Bay (Fig.1). The Mar Grande and the Mar Piccolo basins are joined by means of an artificial channel, i.e. the Navigable Channel, and a natural one, i.e. the Porta Napoli Channel. As shown in Figure 1, along its western side, the Mar Grande is limited by the Cheradi Isles. The North-Western opening between the mainland and the Cheradi Isles is named Punta Rondinella and is about 100m long, while the Southern one between Cheradi Isles and the mainland is about 1400m long.

The total surface area of Mar Grande is about 35 km², while its maximum depth is about 35 m in its central area. Both basins are affected by a polluting charge, being still subjected to different outflows from sources of civil, military, and industrial origins, which are authorized and monitored only in some cases. In the Mar Grande, these discharges are principally located along its northern and north-eastern coastline. Also a submarine freshwater source named citro San Cataldo, with an average flow rate of 17.22 m³/s, is present at the mouth of the Porta Napoli Channel.

In the present study, an extensive set of measured meteorological and biochemical marine data is examined, in order to track some typical features of the basin. These measurements are recorded by a meteo-oceanographic monitoring system installed in the central area of the Mar Grande basin, in the frame of the Flagship Project RITMARE. The system is managed by the research unit of the Technical University of Bari—Department of Civil, Building, Environmental Engineering and Chemistry (DICATECh). Sea waves and currents, meteorological forcings, and water quality indicators are continuously estimated by means of different sensors located in the stationing point. These meteorological and oceanographic data has been recorded since February 2014 over a time period of 11 months, thus allowing us to capture their annual trend and some seasonal features. The digital data has been exported and processed to

produce a synthetic description and to provide the basis for a statistical analysis. In this way, it is possible to correlate the wind action with the wave and current behavior. Moreover, some correlations among the water quality indicators are also deducible.

The aims of the present study are (1) to find a possible correlation between wind and waves, (2) to evaluate the annual trend of selected biochemical indicators, and (3) to deduce the principal behavior of the currents in the investigated area. The paper is structured in the following way: the second section describes the experimental setup, the third section analyzes and discusses winds and wave data; the same is done in the fourth section for physical and biochemical parameters. Finally, currents are debated in the fifth section.



Fig. 1 Target area and location of the monitoring system in the Mar Grande. Source—Google Earth

Observational setup and data analysis

During December 2013, as part of the Flagship Project RITM ARE, with funds from PON R&C 2007-13 Project provided by the Italian Ministry of Education, University and Research, a meteo-oceanographic station was installed in the Mar Grande basin, at the geographical coordinates $40^{\circ} 27, 6' N$ and $17^{\circ} 12, 9' E$ (Fig. 1). The local depth h in this station is on average equal to 23.25 m. The station is provided with many instruments, including a bottom-mounted acoustic Doppler current profiler (ADCP) and a wave array by Teledyne RD, a weather station by Metpack, and different sensors of water physical and

biochemical parameters by WET Labs and Turner Design. In this way, it is possible to collect the time series of a large amount of parameters. In detail, speed and wind direction, air temperature, and relative humidity are measured at a distance of 1.5 m above the sea surface. Sea water temperature, salinity, dissolved oxygen, chlorophyll, chromophoric dissolved organic matter (CDOM), and crude oil are all measured by sensors fixed at a depth on average equal to 5.6 m below the sea surface. Speed and direction of sea currents are measured along the whole water column. In fact the four-beam ADCP, in a Janus configuration, is fixed on the bottom by means of a multipurpose instrument bottom mount, looking vertically upward with the transducer head about 0.50 m above the seafloor. Velocities are sampled along the water column with 0.50 m vertical bin resolution and a 1.60 m blanking distance. Mean current velocity profiles are collected continuously at 1 h intervals, using an average of 60 measurements acquired every 10 s (De Serio and Mossa, 2015). In this way, the analysis allows to derive the hourly averaged velocity components along the water column. Also, the other sensors provide hourly averaged values, with a lower sampling rate. The principal features of the used instrumentations are summed up in Table 1. The large amount of collected data is investigated since February 2014 up to December 2014. In particular, the time series of the hourly recorded signals are examined and when necessary grouped in a monthly base.

Analysis of winds and waves

Being the Mar Grande is a semi-enclosed basin, it was expected that the wave field was dominated by a wind regime which is associated to a growing or wave equilibrium spectrum where peak period waves have phase velocity lower than the wind speed. As the wave energy grows and peak period increases, a point is reached when peak waves have phase speeds larger than the wind and propagate out of the generation region as swells (de Farias et al. 2012). Consequently in the present case, due to the basin topography, wind waves highly correlated with local winds were supposed, with the mean wave propagation not differing significantly from the blowing wind direction. For a wind-sea condition, the direction of wave propagation is expected not to exceed a 90° cone centered in the prevailing wind direction. On the contrary, this condition is not confirmed by our field wind and wave data, as deduced firstly by a comparison, for each investigated month, between the polar charts of the measured winds and of the significant waves. When examining the polar wind distributions, it is deduced that in February, April, and May, dominant winds are north-north-westerly for moderate intensities (5– 10 m/s), while the most intense winds (> 10 m/s) come from S and SE in February and April. In March, a dominance of easterly winds is evident. In June, July, August, and September, wind intensities generally decrease and wind is prevalently from NNE, even if moderate winds from south and north-east are also evident. In September and December, NNW and NE are the prevailing wind directions, while in October winds

from ESE prevail. For the sake of brevity, in Fig. 2, only the polar plots for February, April, June, August, October, and December 2014 are displayed. A stringent correspondence of the wind distribution with the significant wave distribution is not found. Plotted in a polar chart, for each examined month, the significant waves show a propagation direction strictly converging to NE, independently from the prevailing wind direction (Fig. 2). It is worth to remember that along the southwestern boundary of the Mar Grande the wide opening is located (Fig. 1), representing a favorite passage for the significant waves. Therefore, the waves are not strictly locally generated, and their response is more controlled by the topography of the region and by diffraction rather than by transient wind forcing.

In terms of magnitude, to check the response of the wave to the wind speed, their time-varying trends are compared. In February and March, the highest wind speeds are observed (16–18 m/s), as well as the highest significant heights (1.0–1.1 m). The wind intensity reduces in April and May with maxima values in the range 11–13 m/s, while maxima H_s values are around 0.6 m. In June and July, the highest wind intensity is around 10.5 m/s and the highest H_s values are in the range 0.8–0.95 m. The strongest winds in August have intensities below 10 m/s, with highest values of H_s around 0.65 m. Values of highest wind intensities in the range 11–15 m/s are recorded in September, October, November, and December, while the highest values of H_s in the same period are in the range 0.6–0.85 m. The time-varying wind intensities and significant wave heights H_s follow similar trends, but correlations seem to be limited to some peak events.

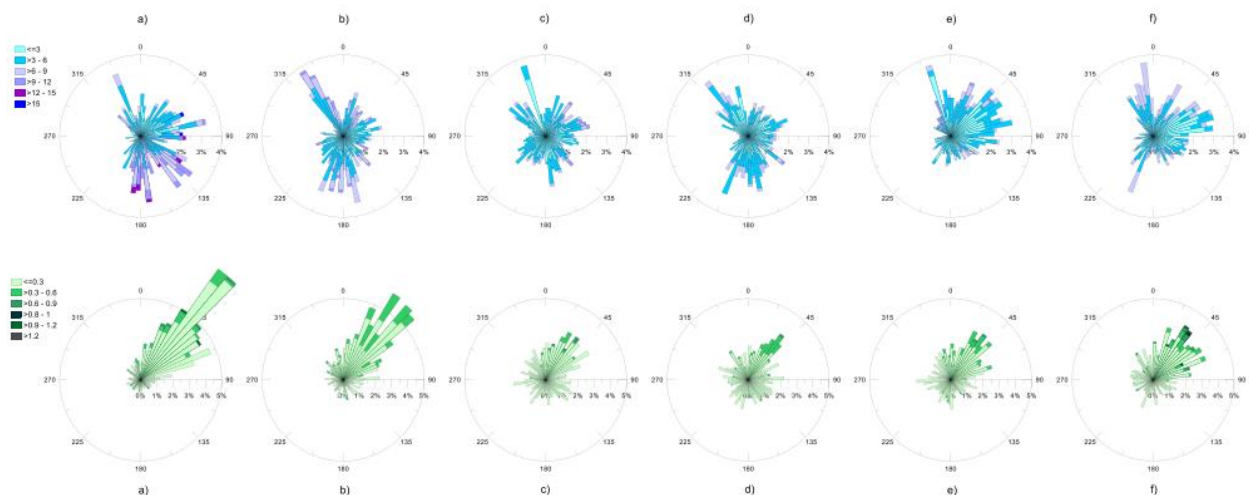


Fig. 2 *Top row:* polar plots of the measured winds during **a** February, **b** April, **c** June, **d** August, **e** October, and **f** December 2014. Directions of provenience shown. *Bottom row:* polar plots of the measured significant wave height during **a** February, **b** April, **c** June, **d** August, **e** October, and **f** December 2014. Directions of propagation shown

To deeply examine this behavior and to assess the fraction of data points corresponding to wind-sea condition, the relation between wind speed, wave height, and wave period is examined. In a wind-generated ocean wave system, the three parameters H_s , peak period T_p , and wind speed U_w are closely

related by the following equation, established through theoretical analysis of wave dynamics and confirmed with several groups of experimental data (Hwang et al. 1998):

$$\frac{U_w}{gT_p} = 0.048 \left(\frac{U_w^2}{gH_s} \right)^{0.67} \quad (1)$$

being g the gravitational acceleration.

Therefore, the measured H_s and T_p were normalized respectively with g/U_w^2 and g/U_w . The scatter plot between $\frac{gH_s}{U_w^2}$ and $\frac{gT_p}{U_w}$ is drawn in a log scale in Figure 3 where all the recorded data is shown.

In this graph, data recorded both in Station O and in Station N are included. It is evident that they tend to collapse in two different lines (dotted lines), far off the fully developed wind-sea curve (solid line). The wind-sea condition represents a very small fraction of the total wave regime in the study region, just about the 6% of the total data. In detail, it is observed that the values of H_s and T_p fitting the wind sea condition are such that their monthly averaged values H_{sm} and T_{pm} provide an dimensionless parameter $H_{sm}/(gT_{pm}^2)$ in the range $0.0025 \div 0.0035$ and an dimensionless parameter $h/(gT_{pm}^2)$ in the range 0.1-0.3. According to Le Meauhtè abacus (Fenton, 1990), these ranges indicate that the significant waves typical of a wind regime are on average Stokes II order waves.

Table 1 Principal characteristics of the instruments located in the monitoring station

Probe	Type	Value
ADCP	Acoustic frequency	600 KHz
	Velocity range	±5 m/s
	Velocity accuracy	0.3 % of the water velocity relative to ADCP ±0.3 cm/s
CTD	Pressure range	0–7000 m
	Pressure accuracy	1‰
	Temperature range	–5 °C–35 °C
	Temperature accuracy	5‰
Submersible fluorometer	Minimum detection limit CDOM	0.15 ppb
	Dynamic range CDOM	0–1250 ppb
	Minimum detection limit CO	0.2 ppb
	Dynamic range CO	0–2700 ppb
ECO sensor	Turbidity sensitivity	0.013 NTU
	Turbidity range	0–25 NTU
	Fluorescence sensitivity	0.025 µg/l Chl
	Fluorescence range	0–50 µg/l Chl

The wave data far off the fully developed wind-sea curve generally have $H_s/(gT_p^2) < 0.0025$ and are best fitted by the two following relations:

$$\frac{U_w}{gT_p} = 0.038 \left(\frac{U_w^2}{gH_s} \right)^{0.49} \quad \text{for } T_p < 10\text{s and } H_s > 0.35\text{m} \quad (2)$$

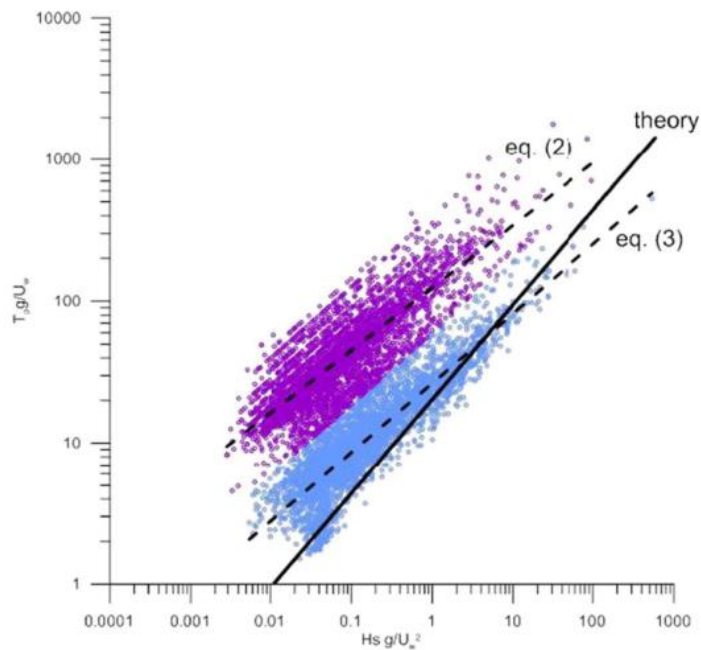
with a regression coefficient equal to $R^2=0.81$ and

$$\frac{U_w}{gT_p} = 0.008 \left(\frac{U_w^2}{gH_s} \right)^{0.44} \quad \text{for } T_p > 10\text{s and } H_s < 0.35\text{m} \quad (3)$$

with a regression coefficient equal to $R^2=0.71$.

Consequently the condition $T_p < 10\text{s}$ sometimes used as a crude method to individuate wind waves and separate them from swells (de Farias et al., 2012) should be considered definitely not exhaustive.

Fig. 3 Relation among wind intensity and significant wave height and period. Solid line represents the theoretical wind-sea relation given by Eq. 1. Dotted lines represent Eqs. 2 and 3, respectively



During the observations, the hourly air and sea surface temperatures (respectively named T_{air} and T) have been recorded, as plotted in Fig. 4a. The atmospheric heat transfer and the sea thermal inertia are evident, with latent and sensible fluxes which tend to cool the sea water in autumn-winter period, when T is greater than T_{air} , while the opposite situation occurs in spring-summer months. Figure 4b shows the scatter plot of the surface water temperature T and salinity S , where the progressive increasing of T is visible, starting with minima values around $13\text{ }^\circ\text{C}$ in autumn- winter months and reaching maxima values around $29\text{ }^\circ\text{C}$ in August. Referring to salinity, its variation during the whole observation period is limited in the range $37.3\text{--}38.5$ psu, with a larger variability in February, March, and April. The analysis of the salinity time series highlights the following. Salinity tends to an average constant value, respectively, of $S = 37.8$ psu in June and July and of $S = 38$ psu in August. These high values recorded are consistent with the typical dry period, characterized by stronger evaporation. In October, November, and December (autumn months) and January, February, March, and April (winter/early spring months), salinity values are generally

lower, around 37.7 psu, even if some peaks also exceeding 38 psu can be clearly distinguished during short time periods. These rapid growths in salinity, temporarily limited, generally occur when the air temperature sharply decreases and a smoothed reduction of the water temperature is also observed. Consequently, this temporary trend could be explained in terms of convective mixing and buoyancy, which lead to a deepening of denser water and a rising of more saline water. However, it is worth remembering that also coastal discharges and land drainage could affect the salinity concentration of the water basin.

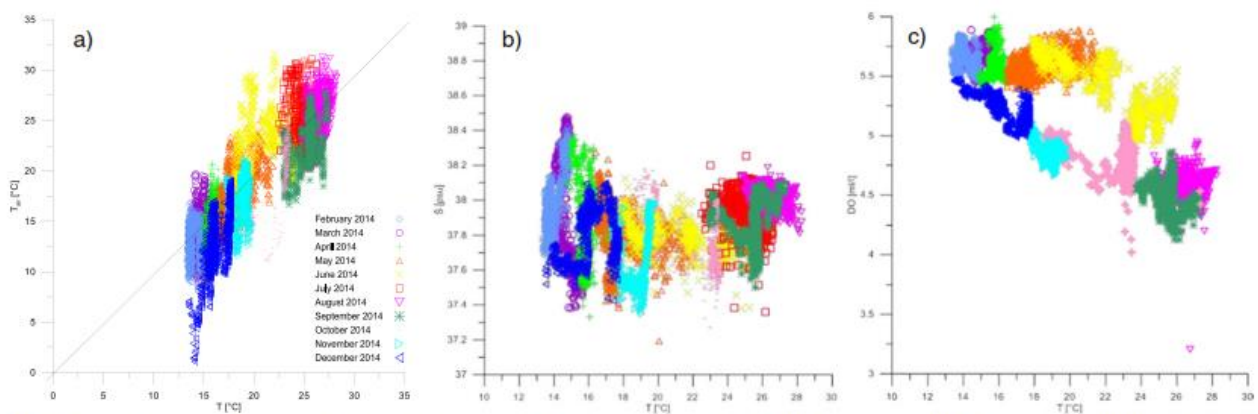


Fig. 4 Scatter plot of sea surface temperature T and, respectively, a air temperature T_{air} , b salinity S , and c dissolved oxygen concentration DO

In order to assess the water quality, the following biochemical parameters are analyzed: dissolved oxygen (DO), chlorophyll (Chl), turbidity, chromophoric (or colored) dissolved organic matter (CDOM), and crude oil (CO) also known as petroleum. They are recorded in the stationing point at a depth on average equal to 5.6 m from the surface, where the sensors are located. Referring to turbidity, indicating the presence of suspended organic and inorganic matter, it affects the light penetration in water and primary productivity, as a consequence. This could be caused by natural factors, wastewater outfalls, and land drainage. Also, the chlorophyll and dissolved oxygen concentrations are strictly connected to primary productivity, considering that they depend on the process of photosynthesis. CDOM is a fraction of the total dissolved organic matter that generally affects water column light penetration and photo-chemical processes. It is the dissolved organic matter in water able of light absorption and is due both to the degradation products of phytoplankton and to the dissolved organic matter from land. It negatively impacts primary productivity because of its light absorption. Crude oil is present in the environment as either emulsions or molecular dissolved oil in water. It can be detected quite easily using fluorescence techniques, because of its chemical structure.

To show the annual variability of the aforementioned parameters, their monthly time series are examined. As an example, Figs. 5–8 show the time series of dissolved oxygen, chlorophyll, and turbidity, grouped in seasonal graphs. It is worth to note that an annual cyclic trend is observed for all these parameters. The dissolved oxygen DO concentration tends to be in the range 5.5–6 ml/l in winter and spring months. In the second half of June, values diminish and reach a concentration of about 4.5 ml/l in August. In autumn, the concentration of DO slightly increases reaching values of 5 ml/l on average and approaching 5.5 ml/l again in December. It is worth to note that the DO concentration depends on the sea surface temperature T (Fig. 4c) and indirectly on the wind mixing more pronounced in autumn-winter season. Moreover, its annual trend, characterized by maxima values in winter (Fig. 5) and minima in summer (Figs. 6 and 7), is consistent with the typical cycle of algal blooms which enhance the oxygen concentration because of the photosynthesis. Also, the oxygen saturation percentage is examined for the whole year, showing that near the surface, where the measurements are recorded, no deficit of oxygen is detected. The chlorophyll concentration trend shows the same behavior of the DO concentration. Its values are around 2 $\mu\text{g/l}$ in February and decrease in spring and summer months (Figs. 5 and 6), converging on average 0.5 $\mu\text{g/l}$. In autumn, the chlorophyll concentration approaches 1 $\mu\text{g/l}$ (Fig. 7) and tends to return to 2 $\mu\text{g/l}$ again in December, when some isolated peaks are also evident (Fig. 8). It is worth to note that the principal source for the chlorophyll concentration in the examined area is represented by the coastal discharges and their consequent outflow of nutrients. In fact, with their progressive closure, a strong reduction of Chl values has been recorded in both the Mar Grande and Mar Piccolo basins (Alabiso et al., 2003). Considering that previous studies focused more on phytoplankton measurements in the investigated area (Caroppo et al. 2014), while a general lack of chlorophyll data is observed, the present long period measurements could be useful to integrate the existing information about the environmental condition of the basin.

Referring to turbidity, it shows values generally lower than 3 nephelometric turbidity units (NTU) in winter months (Fig. 8) and lower than 2 NTU in March–October period (Fig. 5–7). Some turbidity peaks are recorded, as an example, in the last week of August. In any case, they are not connected to rapid salinity changes. Consequently, they could be reasonably explained as the effect of limited and transitory coastal outflows, rather than the effect of rainwater coming from inland. A quite linear correlation is found between turbidity and chlorophyll, so that it increases with increasing chlorophyll and higher values of turbidity are reached in autumn-winter when higher values of chlorophyll are observed likewise (Figs. 7 and 8).

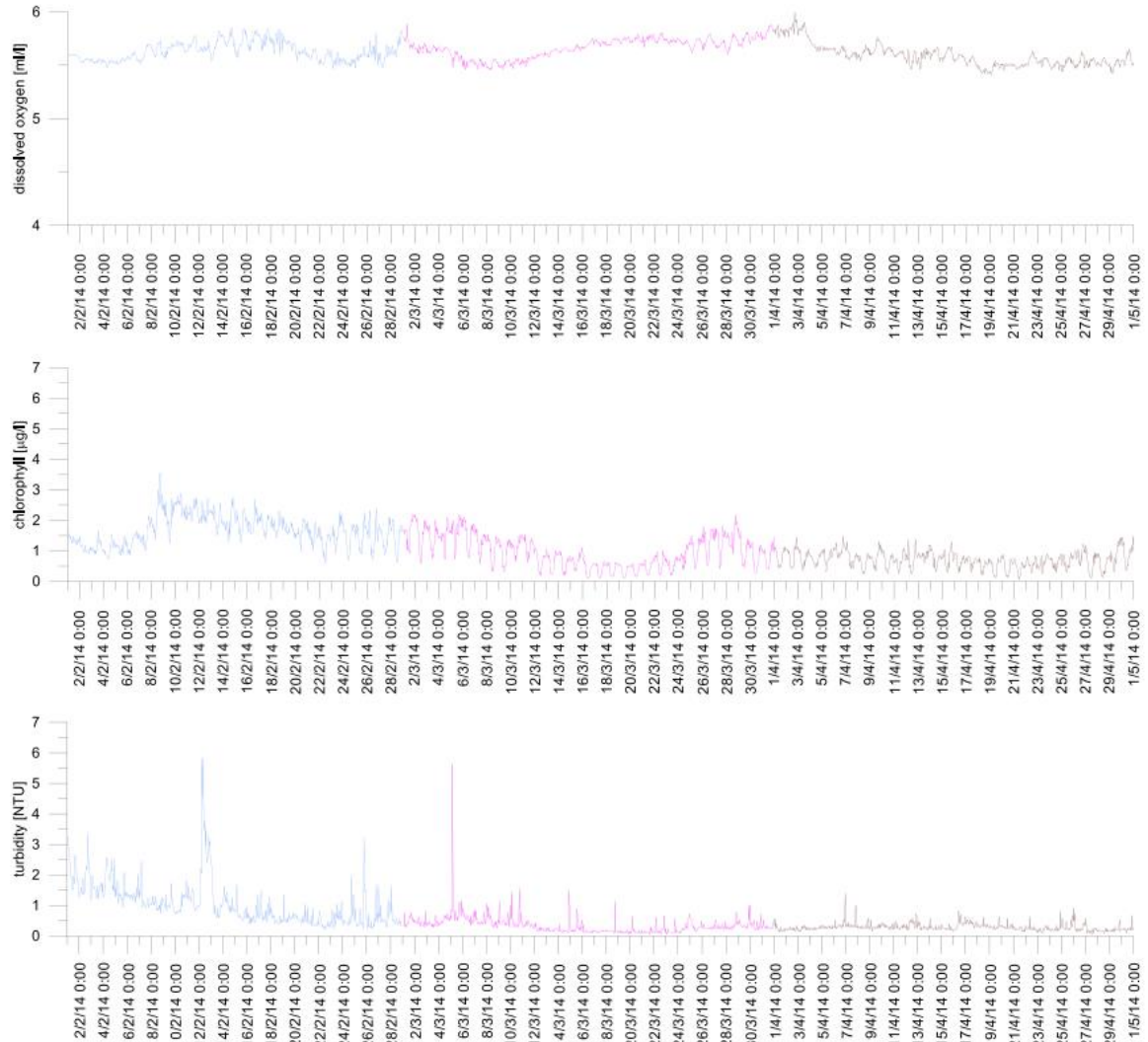


Fig. 5 Time series of dissolved oxygen, chlorophyll, and turbidity, during February, March, and April 2014

The analysis of CDOM highlights the lack of a clear observed relationship between its concentration and chlorophyll concentration and implies that CDOM is not directly released by phytoplankton, in agreement with previous findings in other works (Rochelle-Newall and Fisher 2002). On the contrary, a correlation with the crude oil concentration is recorded, as shown in Fig. 9, where both the CO concentrations and the CDOM concentrations are normalized with their corresponding monthly averaged values (respectively named CO_m and $CDOM_m$). In detail, the fitting relation which better expresses the crude oil concentration as a function of the CDOM concentration is the power function, with a regression coefficient R^2 in the range 0.8–0.9 for each examined month. This result is in agreement with previous experimental data by Huang et al. (2011) and also with numerical modelling results by Huang et al. (2014). It is worth noting that previous direct measurements of hydrocarbons in the basin are very poor, while measurements of hydrocarbons contained in the sediments of the basin are mainly available (Cardellicchio et al. 2006; Annicchiarico et al. 2010). They show that polycyclic aromatic hydrocarbon concentrations

in the sediments of the Mar Grande are higher than admissible values. Consequently, our measured data of CO could contribute to a better knowledge on the distribution and spread of hydrocarbons in the basin.



Fig. 6 Time series of dissolved oxygen, chlorophyll, and turbidity, during May, June, and July 2014

Analysis of currents

Taking into account the bottom fixed ADCP size and its blanking distance, the current velocities are assessed along the vertical starting from $z = 2.1$ m from the sea bed, at constant intervals of 0.5 m (being z the vertical coordinate from the bottom). The examined bins are 38, so that the water column is observed for the whole investigated period up to $z = 20.6$ m. The most superficial layer, with a thickness on average equal to 2.65 m, is excluded from the analysis. In this way, the possible noise in the measurements is filtered out as well as the wave contribution to currents velocity could be considered reduced. Firstly, the current propagation direction is analyzed along the vertical, for each month.



Fig. 7 Time series of dissolved oxygen, chlorophyll, and turbidity, during August, September, and October 2014

As an example, Fig. 10 shows the polar plots of the currents distribution at $z = 2.1$ m (near bottom), at $z = 11.9$ m (mid-depth), and $z = 20.6$ m (near surface) referring to February, April, June, August, October, and December 2014. For each single month, the current direction has an expected variability along the vertical. In any way, with the exception of February and December, in the bin nearest to the bottom, the current is prevalently directed towards SW with intensities more frequent in the range 0.1–0.15. Rarely, bottom current intensities of 0.15–0.2 are also reached. In February and December, the current at $z = 2.1$ m spans clockwise from SW to NNE and is more frequently characterized by smaller intensities in the range 0–0.1. At the intermediate depth $z = 11.9$ m, for each month, currents cover a wide range of directions, with intensities around 0–0.1. In the most superficial bin at $z = 20.6$ m, currents span clockwise from SE to NE during February, April, and June, with episodes of higher current velocity reaching 0.2 m/s and directed to SW, W, and NW. In

August, the superficial current does not show a prevalent direction of propagation, while in October and December, it converges towards directions between SW and NW.

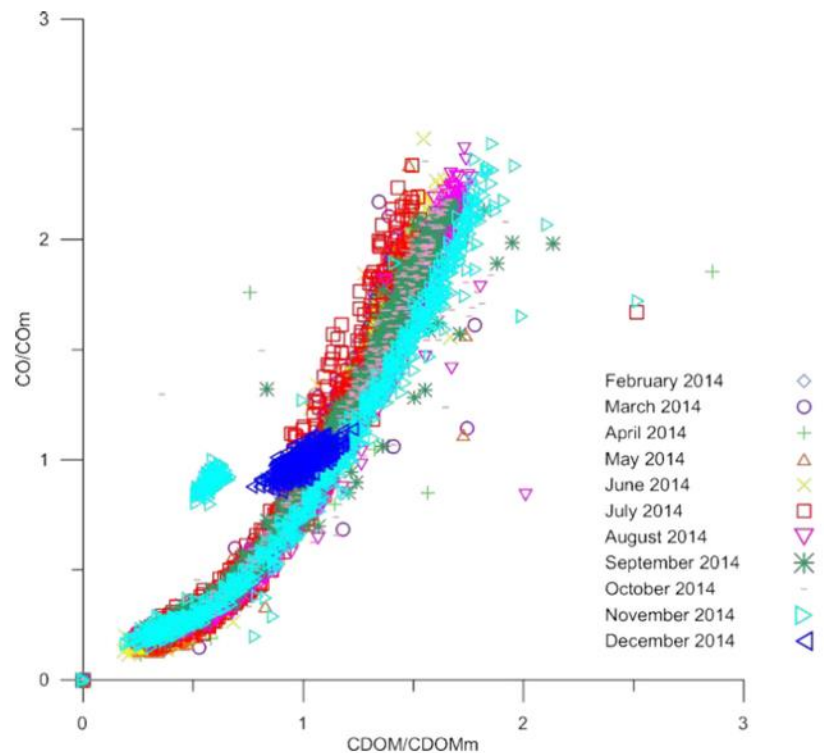


Fig. 8 Time series of dissolved oxygen, chlorophyll, and turbidity, during November and December 2014

The comparison for corresponding months of the polar plots of surface currents (Fig. 10) and significant waves (Fig. 2) reveals that no correlation can be drawn. In fact, as previously written, significant waves generally propagate towards NE, while surface currents show a wide variability in their direction of propagation. More interesting is the comparison of the polar plots of surface currents with those of winds (Fig. 2). In fact, as particularly evident in December, the predominant wind generally seems to feed the surface current, with a slight clockwise shift between leeward winds and propagating currents, which can be consistent with the Ekman effect. As a further confirm, for all the examined months, no westerly winds are recorded as well as rare eastward currents are observed. Due to the limited total local depth, the wind could affect the entire water

column, as also suggested by the calculated Ekman depth, which for moderate winds (5–10 m/s) exceeds 30 m on average. On the contrary, at the intermediate depth $z = 11.9$ m, this relation is no longer evident. Consequently, all the above-described aspects allow us to distinguish in the measuring station the following annual condition. A persistent bottom current is established and is predominantly directed towards SW, while the variable surface current is wind affected. Considering that the significant wave prevalently propagates from SW toward NE, also inducing a water mass transport, the data observed in the measuring station confirms the mass conservation principle.

Fig. 9 Scatter plot of crude oil CO concentration and CDOM concentration, respectively, normalized with their monthly averaged values



In order to better understand the behavior of the superficial currents, the vertical distributions of the velocities assessed in the upper layer ($z = 11.9\text{--}20.6$ m) are analyzed in detail. For each hour, the mean flow direction in this upper layer is detected. Consequently the vertical profiles are evaluated for the velocity component along this direction, the so-called streamwise velocity u_{stream} . Generally, variable values of u_{stream} are evident along the upper water column. In any case, when the dispersion of the velocity with respect to the mean flow direction is slight, the streamwise velocities follow the classic log-law

$$\frac{u_{stream}(z)}{u^*} = \frac{1}{k} \ln \frac{z}{h} + B' \quad (4)$$

being u^* the shear velocity, ν the kinematic viscosity, k the von-Karman's constant equal to 0.41 and B' a function of flow properties and bed roughness (De Serio and Mossa, 2014a). The validity of the log-law for coastal currents has already been proved by De Serio and Mossa (2014a, 2015) in the case of well mixed waters and absent stratification. In the present study, eq. (4) matches the experimental data with the highest values of the regression coefficient, i.e. $R^2=[0.75-0.95]$, in all the cases in which the flow is almost unidirectional in the most superficial layer ($z=16.1\div 20.6\text{m}$). This behaviour further confirms the presence of a superficial mixed layer due to the wind forcing, which deepens till $z=16.1\text{m}$ at least. As an example in Figure 6 some vertical profiles of the streamwise current in the upper layer are shown, referring to February 2014. The fitting log-law is also plotted for each graph.

Conclusions

A large amount of hydrodynamic, physical and biochemical data coming from a bottom fixed meteo-oceanographic station, located in the Mar Grande basin, is analyzed in the present study. Consequently, it is possible to assess some annual typical trends of waves, currents and water quality indicators in this strongly anthropized coastal region. The principal findings can be summed up in the following way.

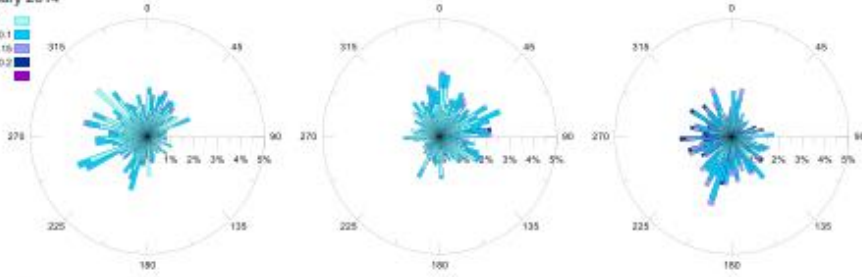
In the investigated period (February–December 2014), the analysis of the wind polar charts shows that the prevailing wind directions of provenience are NNW, S, and SE. A stringent correspondence of the wind distribution with the significant wave distribution is not found. In fact, the significant waves show a propagation direction strictly converging to NE, independently from the blowing wind, thus resulting as more controlled by the topography of the region and the diffraction effect rather than by the transient wind forcing. In the examined annual investigation, a small fraction of the total wave data ($\sim 6\%$) matches the fully developed wind-sea curve. On the contrary, most

wave data tends to collapse in other two curves, experimentally deduced, depending on the wave heights and periods.

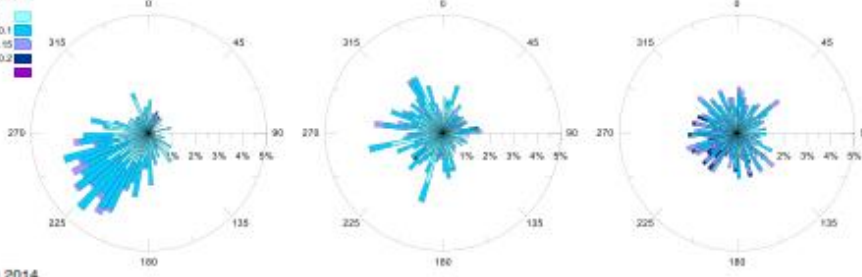
Referring to the physical and biochemical parameters, the analysis of the annual air temperature and sea surface temperature and salinity is consistent with the atmospheric heat transfer, the sea thermal inertia, and the convective mixing. The annual trend of the dissolved oxygen as well as of the chlorophyll concentration is characterized by maxima values in winter and minima in summer, consistently with the typical cycle of algal blooms and photosynthesis. An almost linear correlation is also found between turbidity and chlorophyll. The analysis of CDOM highlights that it is not directly released by phytoplankton. On the contrary, a correlation with the crude oil concentration is recorded, expressed by a power function, in agreement with previous experimental data.

The study of the recorded currents displays that currents are mostly wind induced in the uppermost layer, also according to the Ekman transport. This effect is no longer evident at mid- depth, while near the sea bottom a quasi-steady current directed towards SW is formed. In the superficial layer, the wind mixing is also proved by the calculated vertical profiles of the streamwise velocity, which fit the typical log-law when the flow can be considered unidirectional.

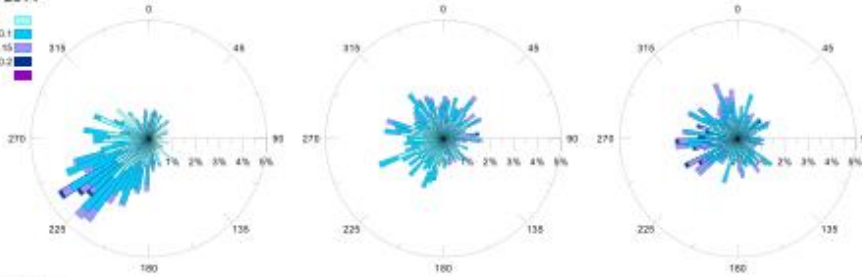
February 2014



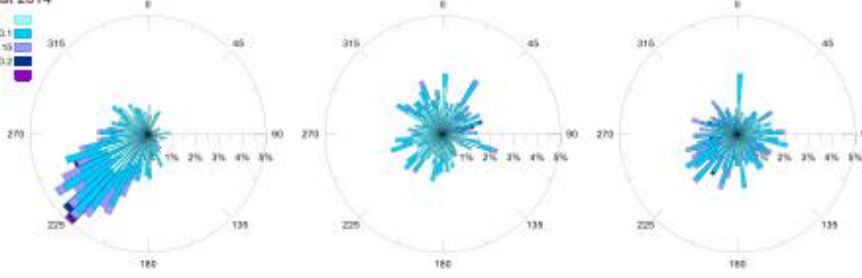
April 2014



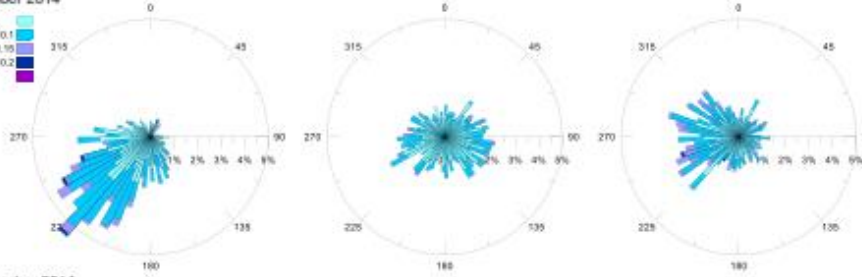
June 2014



August 2014



October 2014



December 2014

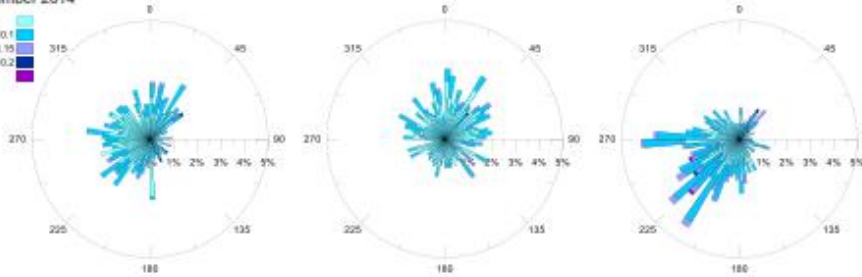


Fig. 10 Current directions near bed at $z=2.1$ m (*left*), at intermediate depth $z=11.9$ m (*center*), and near the surface at $z=20.6$ m (*right*). Directions of current propagation shown

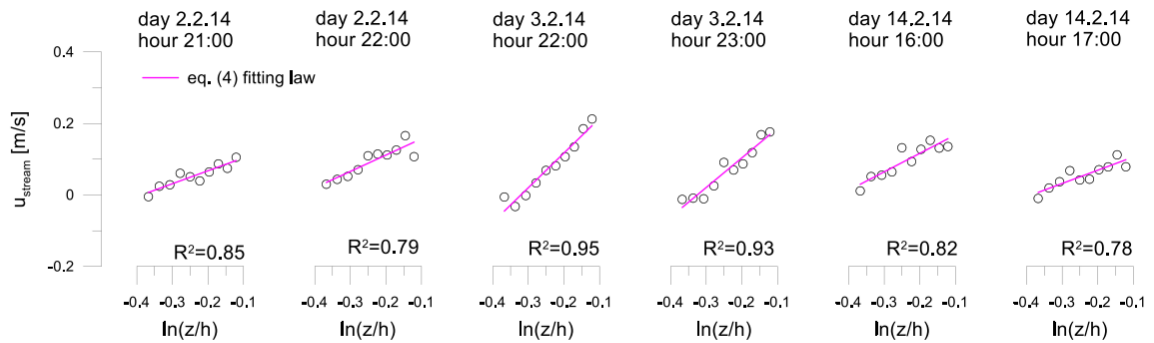


Fig. 11 Streamwise velocity vertical profiles in the superficial layer fitted by the log-law, at some selected times for February 2014

Acknowledgments

The authors acknowledge the support from the Flagship Project RITMARE and from the PON R&C 2007-2013 project, funded by the Italian Ministry of Education, University and Research

References

- Alabiso G, Giacomini M, Milillo M, Ricci P (2003) The Taranto sea system: 8 years of chemical–physical measurements. *Biol Mar Mediterr* 12(1):369–373
- Annicchiarico C, Assennato G, Blonda M, Cardellicchio N, Di Leo A, Giandomenico S, Lopez L, Spada L (2010) Preliminary results of pollutants biomonitoring in coastal marine and transitional waters of Apulia region (Southern Italy). *Fresenius Environ Bull* 19(9):1841–1847
- Cardellicchio N, Buccolieri A, Giandomenico S, Lerario VL, Lopez L, Pizzulli F (2006) Distribution and occurrence of polycyclic aromatic hydrocarbons (PAHs) in sediments from the Mar Grande and Gulf of Taranto (Ionian Sea, Southern Italy). *Ann Chim* 96(1–2):51–64

- Caroppo C, Musco L, Stabili L (2014) Planktonic assemblages in a coastal Mediterranean area subjected to anthropogenic pressure. *J Geogr Nat Disast* 4:121
- de Farias EGG, Lorenzetti JA, Chapron B (2012) Swell and wind-sea distributions over the mid-latitude and tropical north Atlantic for the period 2002–2008. *Int J Oceanogr* 306723:1–8
- De Serio F, Mossa M (2014a) Streamwise velocity profiles in coastal currents. *Environ Fluid Mech* 14(4):895–918
- De Serio F, Mossa M (2014b) Monitoring and modelling of coastal currents and wastewater discharge: A case study. *Geo Eco Marina* 20
- De Serio F, Mossa M (2015) Analysis of mean velocity and turbulence measurements with ADCPs. *Adv Water Resour* 81:172–185. doi:10.1016/j.advwatres.2014.11.006
- De Serio F, Malcangio D, Mossa M (2007) Circulation in a Southern Italy coastal basin: modelling and field measurements. *Cont Shelf Res* 27: 779–797
- Di Leo A, Annicchiarico C, Cardellicchio N, Giandomenico S, Spada L (2013) Trace metal distributions in *Posidonia oceanica* and sediments from Taranto Gulf (Ionian Sea, Southern Italy). *Mediterr Mar Sci* 14(1):204–213
- Fenton JD (1990) Nonlinear wave theories. In: Le Méhauté B, Hanes DM (eds) *The sea—ocean engineering science, part A, vol 9*. Wiley, New York
- Huang M, Xing X, Song Q, Shen Z (2011) The retrieval model for organic contamination in waters using optical absorption properties of C-DOM. 34 Int. Symposium on Remote Sensing of Environment, 10–15 April, Sydney, Australia
- Huang M, Xing X, Zhao Z, Li Z (2014) Dynamic monitoring of water petroleum substance using HJ-1/CCD remote sensing data. *IOP Conf. Series: Earth and Environmental Science*, 17. doi:10.1088/1755-1315/17/1/012104

Hwang PA, Teague WJ, Jacobs GA, Wang WD (1998) A statistical comparison of wind speed, wave height and wave period derived from satellite altimeters and ocean buoys in the Gulf of Mexico region. *J Geophys Res* 103:10451–10468

Mossa M (2006) Field measurement and monitoring of wastewater discharge in sea water. *Estuar Coast Shelf Sci* 68:509–514

Rochelle-Newall EJ, Fisher TR (2002) An investigation into phytoplankton as a source of chromophoric dissolved organic matter. *Mar Chem* 77:7–21

Scroccaro I, Matarrese R, Umgiesser G (2004) Application of a finite element model to the Taranto Sea. *Chem Ecol* 20:205–224.